PROCEEDINGS, Thirty-First Workshop on Geothermal Reservoir Engineering
Stanford University, Stanford, California, January 30-February 1, 2006
SGP-TR-179

WELL TEST ANALYSIS FOR NATURALLY FRACTURED RESERVOIRS WITH TRANSIENT INTERPOROSITY MATRIX, MICROFRACTURES, AND FRACTURES FLOW

Héctor Pulido [1], Fernando Samaniego V. [2], Jesús Rivera [2], Felipe Díaz [2], and Guadalupe Galicia[3]

1. Pemex, 2. National University of Mexico, 3. IMP.
Facultad de Ingeniería
México, D. F, 04510, México
ance@servidor.unam.mx

ABSTRACT

Constant flow, rate solutions are presented for a fractured reservoir with transient interporosity flow in a convolution form, considering matrix, microfractures, and fractures flow.
New solutions are presented for two cases, where there is no primary flow through the microfractures and where the compressive and distensive strength process has created an interconnected system of microfractures. In both cases there is an interaction between matrix, microfractures, and fracture systems.
The numerical inversion was carried out with Stehfest's algorithm. In addition, approximate analytical solution for short and long dimensionless time are obtained and compared with the solution obtained by numerical inversion, providing satisfactory results. The values of the numerical inversion were used to generate the "type curve", presented in terms of the dimensionless groups derived from the approximate analytical solution.

Introduction

In areas lacking cores, open-hole wireline logs may be used to help identify microfractures zones; however, microfractures are not always recognized by conventional logs because of their limited vertical resolution.
Microfractures porosity is common in many reservoirs, and its importance in the petrophysical and productive characteristics of a rock has been recognized by several authors.
Microfracture porosity can be subdivided into connected and disconnected types. Microfractures effect on permeability is related to their connectivity. High permeability may be present in microfractures zones by solution enhancement of pore throats that creates an interconnected system of microfractures. The presence of high-porosity and high-permeability microfractures zones may diminish gasflood effectiveness and leave a large amount of bypassed fluids in the lower permeability matrix. One purpose of our work is to present a technique to identify high secondary porosity, mainly microfractures porosity.
It has been observed in the literature that microfracture zones strongly influence production performance. The present addresses the problem of modeling microfractures in naturally fractured reservoirs, allowing the possibility of primary flow through microfractures, and develops a method to identify microfractures in reservoirs through well tests and decline curves analysis, evaluating porosity associated with microfractures and fractures, and determining microfractures connectivity.
The proposed model can be used to elaborate numerical simulators. Some comparisons between results of analytical solutions derived in this work, and those obtained with a numerical simulator that uses the proposed model are presented.

Background

Dual porosity simulators consider only the matrix and fracture systems, where fluids are produced through the fracture system.
The permeability of naturally fractured rocks is related to the amount of interparticle porosity, amount of separate microfracture porosity, the presence or absence of fractures, and the presence or absence of touching microfractures. Touching microfractures contribute to both effective porosity and permeability.
A triple-porosity single-permeability model was first proposed by Abdassah and Ershagi. These authors considered an unsteady-state interporosity flow model between the fracture system, with two types of matrix blocks, and primary flow only through the fracture system.
In order to use a double-porosity simulator to study the behavior of naturally fractured, with microfractures reservoir, it is required that matrix, fracture, microfractures reservoirs, it is required that matrix, fractures, and microfractures porosities be partitioned into primary and secondary porosities. The connected microfractures have to be treated as fractures in the numerical model, while the rest of the microfractures can be treated as isolate microfractures and included into the matrix porosity, as additional porosity.
Of course, one of the challenges of modeling these reservoirs in this way is the determination of the percent of microfractures connected to the fractures and that

connected to the matrix. Microfractures interact with both matrix and fracture systems.
The porosity and permeability of microfractures and fractures systems may be very different and lead to dominance of the overall response by processes in one of the two systems at different times. Also, fractures always occupy a very small portion of the reservoir volume, while porosities as high as 28% corresponding to intervals having secondary microfractures porosity can be found.
Thus, it is important to recognize microfractures porosity so that accurate reservoir properties can be derived, resulting in less bypassed fluids and higher proven reserves. For these reasons, it is necessary to distinguish between these two void systems, and to model their behavior as two separate but interacting systems.
In highly microfractured naturally fractured reservoirs some microfractures could be closed, containing fluids even below the fluid-water-contact, as the fluids may have been trapped during migration and flow channels may have been sealed due to post-migration tectonic.
Herrera et. al. reported microfracture compressibility to be approximately six times that of the matrix. Considering that pore volume compressibility is a major energy source for microfractures in naturally fractured reservoirs, it is also necessary to distinguish between microfractures and matrix as separate but interacting systems.
It is important to establish a triple porosity model, allowing an interaction between matrix, microfractures, and fractures, where primary flow occurs only through the fracture network.
Using x-ray computed tomography Casar and Suro[1] found that porosity and permeability enhancement may be due to microfractures directly connected, and to microfractures connected through zones of slightly enhanced matrix porosity and permeability surrounding them. These halos are concentric around microfractures, and their porosity decrease from the microfractures centers to the extremes. Values as high as 700 md were measured in the halos around the microfractures, whereas lower values were measured for the regions of the core farther away from the microfractures.
This difference in values suggests that the microfractures are interconnected to some degree through their halos. In fact, in some cases even fractures may be present, they are considered secondary in their effect on permeability in the microfractures zones.
Some simple model has been proposed to evaluate microfractures permeability.
Microfracture permeability in some reservoirs is very important. In fact, in some cases it is more important than fracture permeability. It is common to find that microfracture permeability of 3-5.5 Darcy was assigned to build different models.
As Quintero et. al. explained, NMR tools will respond primarily to matrix permeability and will be insensitive to the dramatic influence on total permeability of open fractures or well-connected microfractures.
A double porosity-double permeability model was first presented by Bourdet. This model uses the Cinco and Samaniego idealization, but allowing primary flow through the matrix.
It is pertinent to establish a triple porosity model, allowing an interaction between matrix, microfractures, and fractures, but beside having flow through the fracture, also including the possibility of having primary flow through the system of microfractures. Thus, this model would be a triple porosity-dual permeability model.

Results
This section is divided in two parts. The first part presents the formulation of the model. The second part presents the pressure behavior during the transient period, for both dual and single-permeability models.

Model Formulation
In this work, a triple porosity model-dual permeability is proposed using the transient interporosity flow, and a skin between the two media the model the matrix-secondary fractures and fractures, that could result in pseudosteady interporosity flow. The pseudosteady fluid transfer between matrix, microfractures, and fractures systems is directly proportional to the difference in the volume average macroscopic matrix, microfractures, and fractures pressure. A free interaction between matrix, microfractures, and fractures systems is allowed when the skin is zero between two media. This is different from the model proposed by Abdassah and Esshaghi, and for this reason the triple porosity model proposed in this work is unique.
Radial flow in the *large* scale secondary porosity media with two source terms in convolution form is described in dimensionless variables, for the triple porosity-dual permeability model, as follows:

$$\kappa\left[\frac{\partial p_{FD}(r_D,t_D)}{\partial r_D^2}+\frac{1}{r_D}\frac{\partial p_{FD}(r_D,t_D)}{\partial r_D}\right]$$
$$-\omega_f C_{mfbD}\frac{\partial p_{FD}(r_D,t_D)}{\partial \tau}*\frac{F_{fF}(\eta_{fD},t_D)}{1+S_{fF}F_{fF}(\eta_{fD},t_D)}$$
$$-\left[1-\omega_F-\omega_f\right]C_{mFbD}\frac{\partial p_{FD}(r_D,t_D)}{\partial \tau}*\frac{F_{mF}(\eta_{mD},t_D)}{1+S_{mF}F_{mF}(\eta_{mD},t_D)}$$
$$=\omega_F\frac{\partial p_{FD}(r_D,t_D)}{\partial t_D} \qquad (1)$$

Where F_{mF} and F_{fF} are the source functions for matrix and microfractures.

Transient matrix-fracture linear flow:

$$F_{mF}(\eta_{mFD},t_D-\tau)=4\eta_{mFD}\sum_{n=0}^{\infty}e^{-\eta_{mFD}(2n+1)^2\pi^2(t_D-\tau)}d\tau \qquad (2)$$

Transient microfractures-fractures linear flow:

$$F_{fF}\left(\eta_{fFD},t_D-\tau\right)=4\eta_{fFD}\sum_{n=1}^{\infty}e^{-\eta_{fFD}(2n+1)^2\pi^2(t_D-\tau)}d\tau \qquad (3)$$

Initial condition:

$$p_{fD}(r_D,0)=0 \qquad (4)$$

Internal boundary condition: constant flow rate

$$\frac{\partial p_{FD}(1,t_D)}{\partial r_D}=-1\cdot \qquad (5)$$

External boundary condition: Infinite reservoir

$$\lim_{r_D\to\infty}p_{fD}(r_D,t_D)=0. \qquad (6)$$

Radial flow in the *small* scale secondary porosity (microfractures) is given by:

$$[1-\kappa]\left[\frac{\partial p^2{}_{fD}(r_D,t_D)}{\partial r_D^2}+\frac{1}{r_D}\frac{\partial p_{fD}(r_D,t_D)}{\partial r_D}\right]$$
$$-\omega_F C_{fFbD}\frac{\partial p_{fD}(r_D,t_D)}{\partial\tau}*\frac{F_{fF}(\eta_{fD},t_D)}{1+S_{fF}F_{fF}(\eta_{fD},t_D)}$$
$$[1-\omega_f-\omega_F]\left[C_{mfbD}\frac{\partial p_{fD}(r_D,t_D)}{\partial\tau}*\frac{F_{mf}(\eta_{mD},t_D)}{1+S_{mf}F_{mf}(\eta_{mD},t_D)}\right]$$
$$=\omega_f\frac{\partial p_{fD}(r_D,t_D)}{\partial t_D} \qquad (7)$$

The transient linear flow matrix-microfracture transfer:

$$F_{mf}\left(\eta_{mfD},t_D-\tau\right)=4\eta_{mfD}\sum_{n=0}^{\infty}e^{-\eta_{mfD}(2n+1)^2\pi^2(t_D-\tau)}d\tau. \qquad (8)$$

Initial condition:

$$p_{FD}(r_D,0)=0. \qquad (9)$$

Internal boundary condition: constant flow rate

$$\frac{\partial p_{FD}(1,t_D)}{\partial r_D}=-1. \qquad (10)$$

External boundary condition: Infinite reservoir

$$\lim_{r_D\to\infty}p_{FD}(r_D,t_D)=0. \qquad (11)$$

The porosities are defined by:

Small scale secondary porosity:

$$\phi_{fb}=\frac{V_{pf}}{V_b}; \qquad (12)$$

Large scale secondary porosity:

$$\phi_{Fb}=\frac{V_{pF}}{V_b}; \qquad (13)$$

Matrix porosity when uses the reference bulk rock:

$$\phi_{mb}=\frac{V_{pm}}{V_b} \qquad (14)$$

Intrinsic matrix porosity:

$$\phi_m=\frac{V_{pm}}{V_m} \qquad (15)$$

Extension of Van Golft Rach definition for the intrinsic matrix porosity, ϕ_m:

$$\phi_m=\phi_{mb}[1-\phi_{Fb}-\phi_{fb}] \qquad (16)$$

Matrix area exposed to large scale secondary porosity:

$$C_{mFb}=\frac{A_{mF}}{V_b} \qquad (17)$$

Matrix area exposed to small scale secondary porosity:

$$C_{mfb}=\frac{A_{mf}}{V_b} \qquad (18)$$

Microfracture area exposed to large scale secondary porosity:

$$C_{fFb}=\frac{A_{fF}}{V_b} \qquad (19)$$

Interporosity flow shape factor between medium *i* and medium *j*.

$$\sigma_{ij}=\frac{A_{ij}}{V_b l_{cij}}=\frac{C_{ijb}}{l_{cij}} \qquad (20)$$

where the dimensionless variables are given by

$$r_D=\frac{r}{r_w} \qquad (21)$$

$$t_D=\frac{[k_{Fb}+k_{fb}]t}{\left[\phi_{Fb}c_{tFb}+\phi_{mb}c_{tmb}+\phi_{fb}c_{tfb}\right]\mu r_w{}^2} \qquad (22)$$

$$p_{FD}=\frac{2\pi[k_{Fb}+k_{fb}]h[p_i-p_F(r,t)]}{qB\mu} \qquad (23)$$

$$p_{mD}=\frac{2\pi[k_{Fb}+k_{fb}]h[p_i-p_m(r,t)]}{qB\mu} \qquad (24)$$

$$p_{fD}=\frac{2\pi[k_{Fb}+k_{fb}]h[p_i-p_f(r,t)]}{qB\mu} \qquad (25)$$

The storativity ratios, for fractures and microfractures are given, by,

$$\omega_F = \frac{\phi_{Fb} c_{tFb}}{\phi_{Fb} c_{tFb} + \phi_{mb} c_{tmb} + \phi_{fb} c_{tfb}} \quad (26)$$

$$\omega_f = \frac{\phi_{fb} c_{tfb}}{\phi_{Fb} c_{tFb} + \phi_{mb} c_{tmb} + \phi_{fb} c_{tfb}} \quad (27)$$

$$\lambda_{mF} = \sigma_{mF} k_m r_w^{\,2} / [\, k_{Fb} + k_{fb} \,] \quad (28)$$

$$\lambda_{mf} = \sigma_{mf} k_m r_w^{\,2} / [\, k_{Fb} + k_{fb} \,] \quad (29)$$

$$\lambda_{fF} = \sigma_{fF} k_{fF} r_w^{\,2} / [\, k_{Fb} + k_{fb} \,] \quad (30)$$

with $k_{fF} = k_f$ if $p_f > p_F$, and $k_{fF} = k_F$ otherwise.

The ratio of the bulk permeabilities of the fractures (large scale) to the total $(k_{Fb} + k_{fb})$, k, is defined as:

$$\kappa = \frac{k_{Fb}}{k_{Fb} + k_{fb}} \quad (31)$$

Note that in the definitions of λ_{mF} and λ_{mf}, we have used the matrix permeability k_m because we expect that under production conditions fluid goes from matrix to microfractures and fracture networks.

For the case of the triple porosity-single permeability model, i.e. when there is only primary flow through the fractures or through the microfractures network, the microfractures and fractures permeability, in the above definitions is set equal to zero except in the numerator of λ_{fF}. For these cases $\kappa = 1$ and 0, respectively.

Dimensionless matrix area exposed to large scale secondary porosity:

$$C_{mFbD} = \frac{C_{mFb} l_c V_b}{V_m} = \frac{A_{mF} l_{cmF}}{V_m} \quad (32)$$

Dimensionless matrix area exposed to small scale secondary porosity:

$$C_{mfbD} = \frac{C_{mfb} l_c V_b}{V_m} = \frac{A_{mf} l_{cmf}}{V_m} \quad (33)$$

Dimensionless microfracture area exposed to large scale secondary porosity:

$$C_{fFbD} = \frac{C_{fFb} l_c V_b}{V_m} = \frac{A_{fF} l_{cfF}}{V_m} \quad (34)$$

$$\eta_{fFbD} = \frac{\eta_{fb} r_w^2}{\eta_{Fb} \varsigma^2} = \frac{k_{fb} (\phi c_t)_t r_w^2}{k_{Fb} (\phi c_t)_{fb} \varsigma^2} = \frac{(\phi c_t)_t \lambda_{fF}}{12 (\phi c_t)_{fb}}$$

$$\eta_{mFbD} = \frac{\eta_{mb} r_w^2}{\eta_{Fb} \varsigma^2} = \frac{k_{mb} (\phi c_t)_t r_w^2}{k_{Fb} (\phi c_t)_{mb} \varsigma^2} = \frac{(\phi c_t)_t \lambda_{mF}}{12 (\phi c_t)_{mb}}$$

$$\eta_{mfbD} = \frac{\eta_{mb} r_w^2}{\eta_{fb} \varsigma^2} = \frac{k_{mb} (\phi c_t)_{fb} r_w^2}{k_{fb} (\phi c_t)_{mb} \varsigma^2} = \frac{(\phi c_t)_{fb} \lambda_{mf}}{12 (\phi c_t)_{mb}}$$

Appendix A presents the solution in the Laplace space for the triple porosity single permeability model, considering constant flow rate and an infinite reservoir.

Transient Well Test Behavior

It is shown that the solution given by Eqs. (A-16) or (A-17), extends the typical Warren and Root (1963) solution. Figures 1-3 present analytical results obtained by applying Stefhest algorithm (1970) to Eq. (A-16) for different values of the parameters λ_{mF}, λ_{fF} y λ_{mf}, ω_F, and ω_f, considering that wellbore storage and skin are zero. In all cases the Cinco and Samaniego (1982) solution with $S_{mf} \approx 10$ (Warren and Root) is represented by the continuous line. At early times a semilog straight line can be observed. The presence of an early semilogarthmic straight line indicates the fractures-controlled flow period.

At late times, a straight line parallel to the early-time line represents the homogenous flow period of the matrix, microfractures, and fractures, where pressure in fractures, microfractures, and matrix, is the same (see Fig. 4).

In a most curves, presented in Figs. 1-3, there are anomalous slope changes during the transition period, caused by the presence of microfractures. In some cases, another intermediate straight line, parallel to the above straight lines, is present during this transition period.

This behavior is different from the double-porosity response. Before and after this intermediate straight line there are transition periods, whose slopes may be different from the characteristic constant pressure drop period of Warren and Root. During these transition periods, apparent straight lines may be fitted, with slope ratios that could be 2:1 for the early, intermediate, or late-time segments, which could be interpreted as a transient interaction between matrix and fractures, especially if one of the three parallel straight lines is missing because of wellbore storage effects, or because of the short duration of the test.

The duration of the anomalous slope changes during the transition period is a function of $\lambda_{fF} / \lambda_{mF}$ and $\lambda_{mf} / \lambda_{mf}$.

Figure 4 presents a comparison of fractures and microfractures pressure profiles, at different times, obtained with a finite difference numerical simulator, which considers the mathematical formulation presented in this work. We can observe an excellent agreement between analytical and numerical results.

As expected before the homogeneous flow period, microfractures pressure drop profiles around the wellbore are lower than fracture profiles. The matrix profiles, not shown in this figure, before the homogeneous period is very small. During the homogeneous flow period, fracture, microfractures, and matrix pressure profiles agree. Although profiles computed with the complete analytical solution, given by Eq. (A-23) are not presented in this figure, they are very close to the numerical profiles.

Using the analytical solution, given by Eq. (A-14), short, intermediate, and long time approximations are obtained. The asymptotic behaviors predicted by these expressions are shown in Fig. 5, for two cases of microfractures.

The number of variables to be defined, three interporosity flow parameters, three interporosity flow parameters, two storativity ratios, wellbore storage constant, and skin factor, makes the use of a type curve matching procedure necessary. Figures 6 and 7 show two type curves for un connected microfractures, with $\lambda_{mf} = 10^{-7}, \omega_F = 10^{-5}$, and considering no wellbore storage and skin effects.

Fig. 6 includes pressure and pressure derivative curves for different values of λ_{mF} and ω_f, for a constant λ_{fF} of 10^{-7}, are presented. In Fig. 7, the parameters λ_{fF} and ω_f are varied and $\lambda_{mF} = 10^{-7}$. In both figures we observe a change of slope during the transition period, that shows in the pressure derivative as two "dips", which is not present in typical double-porosity type curves.

As explained in the Background section, permeability may be enhanced through the connection of microfractures. This solution, that also includes a skin in both microfractures and fractures, extends the single permeability solution. The inclusion of microfractures skin factor is important, because well-connected large microfractures are usually invaded by drilling mud.

Figures 8 and 9 present results obtained by using Sthefest algorithm for different values of the parameters: κ, λ_{mF}, λ_{fF}, λ_{mf}, ω_F, and ω_f, considering that wellbore storage and skins are zero. In all cases the Warren and Root solution is represented by the continuos line without symbols. The more general solution that includes the microfractures is given by Eq. (A-16). At early times no well defined semilog straight line can be observed for the connected microfracture cases. This is in agreement with the findings of Gringarten (1979) for the case of double porosity-double permeability. At late times, a straight line corresponding to the homogenous flow period of fractures, microfractures, and matrix, is present. In general, before the homogeneous flow period, the behavior is different when primary flow through the microfractures network is allowed, being more dramatic this difference when ω_f is big as it is in Fig. 9. As the parameter κ decreases, keeping the rest fixed, the solution loses its characteristic fractured reservoir and it tends to the homogeneous one.

Figure 10 shows a comparison of pressure profiles of fractures and microfractures obtained with a numerical simulator. Comparing these results with those of Fig. 4, we observed that when microfractures are connected, the fracture and microfractures pressure at the sandface is the same, when skin in both fractures and microfractures are zero. The analytical solution, presents a very good agreement with the numerical profiles. This is a verification of both numerical and analytical solutions.

We observe that expressions derived in the present paper, can predict the behavior at early times, which may be of practical interest. The long time approximation for this case will be similar to that of unconnected microfractures.

For connected microfractures, is even more necessary the use of a type curve matching technique to find all the parameters that control the response.

Even the type curve matching procedure may be difficult and not unique, it represents an attractive possibility to obtain the distribution of porosity between fractures, microfractures, and matrix, and their interaction. This is important because core data underestimate the permeability of microfractures zones, and microfractures are not always recognized by conventional logs.

CONCLUSIONS

The main purpose of this work has been to present a more general transient test analysis for NFR based on the transient interporosity flow, including the matrix and microfracture skin effect.

From the results of this study, the following conclusions can be established:

- Approximate analytical solutions for short and long times are presented; others previously presented solutions are particular cases.
- The fracture parameters of permeability and storativity can be estimated through the methodology of this study.
- The estimated flow rate considering transient matrix to fractures transfer, and transient microfracture to fracture transient obtained in this work, is higher than the value of pseudosteady state given by Rodriguez de la Garza et. al.

REFERENCES

Adams, A. R., Ramey, H. J., Jr. and Burguess, R. J., 1968: "Gas Well Testing in a Fractured Carbonate Reservoir", *JPT* (Oct.) 1187-1194; *Trans*., AIME **243**.

Barenblatt, G. I. and Zheltov, Iu., 1960: "Fundamental Equations of Filtration of Homogeneous Liquids in

Fissured Rocks" (in Russian), Soviet Physics Doklady, **Vol. 5**, 522-525.

Barenblatt, G. I., Zheltov, Iu. P. and Kochina, I. N., 1960: "Basic Concepts in the Theory of Seepage of Homogeneous Liquids in Fissured Rocks"**,** *Journal* Applied Mathematical and Mechanics, **24** (5), pp. 1286-1303.

Bourdet, D. and Gringarten, A. C., 1980: "Determination of Fissure Volume and Block Size in Fractured Reservoirs by Type Curve Analysis", paper SPE 9293 presented at the 55th Annual Technical Conference and Exhibition, Dallas, Tex., Sep. 21-24.

Chen, C. C., Serra, K., Reynolds, A. C. and Raghavan, R., 1985: "Pressure Transient Analysis Methods for Bounded Naturally Fractured Reservoirs", *SPEJ* (June), 451-464.

Cinco Ley, H. and Samaniego, V. F., 1982: "Pressure Transient Analysis for Naturally Fractured Reservoirs", paper SPE 11026. presented at the 57th Annual Fall Technical Conference and Exhibition New Orleans, La., September 26-29.

Cinco Ley H., Samaniego, V. F and Kucuk, F., 1985: "The Pressure Transient Behavior for a Naturally Fractured Reservoirs with Multiple Block Size", paper SPE 14168 presented at the Annual Technical Conference and Exhibition, Bakersfield, CA., March 27-29.

Crawford, G. E, Hagedorn, A. R. and Pierce, A. E., 1976: "Analysis of Pressure Buildup Tests in a Naturally Fractured Reservoir", *J. Pet. Tech*. (Nov.) 1295-1300.

Da Prat, G., Cinco-Ley, H. and Ramey, H. J. Jr., 1981: "Decline Curve Analysis Using Type Curves for Two Porosity System"**,** *SPEJ* (June), 354-362.

Da Prat, G., Ramey, H. J., Jr. and Cinco-Ley, H., 1981: "A Method to Determine the Permeability-Thickness Product for a Naturally Fractured Reservoirs", paper SPE 9906 presented at California Regional Meeting, Bakersfield, CA. March 25-26.

Ehlig-Economides, C. A., 1979: "Well Test Analysis for Wells Produced at a Constant Pressure"**,** Ph. D dissertation, Stanford, University Stanford, Calif.

Fetkovich, M. J., 1980: "Decline Curve Analysis Using Type Curves", *J. Pet. Tech.* (June), 1065-1077.

Gringarten, A. C. and Witherspoon, P. A., 1972: "A Method of Analyzing Pumping Test Data from Fractured Aquifer", Proc. Symp. Percolation Fissured Rock, Int. Soc. Rock Mech., Stuttgart T3, b-1-b9.

Gringarten, A., C., 1979: "Flow Tests Evaluation of Fractured Formations", paper presented at the symposium on Recent Trends in Hydrogeology. Berkeley, CA, Feb. 8-9.

Gringarten, A. C., Burgess, T. M., Viturat, D., Pelisser, J. and Aubry, M., 1981: "Evaluating Fissured Formation Geometry from Well Test Data: A Field Example", paper SPE 10182 presented at the 56th Annual Technical Conference and Exhibition, San Antonio, Texas, Oct. 5-7..

Gringarten, A. C., 1982: "Interpretation of Tests in Fissured Reservoirs and Multilayered with Double Porosity Behavior: Theory and Practice", paper SPE 10044, presented at International Petroleum Exhibition and Technical Symposium, Beijing, China, March 26-28.

Jacob, C. E. and Lohman, S. W., 1952: "Nonsteady Flow to a Well of Constant Drawdown in an Extensive Aquifer", *Trans*. Am. Geophys. Union (August) 559-569.

Kazemi, H., 1969: "Pressure Transient Analysis of Naturally Fractured Reservoirs with Uniform Fracture Distribution", *Soc. Pet. Eng. J*. (Dec.), 451-462; *Trans*. AIME, **246.**

Kucuk, F. and Sawyer, W. K., 1980: "Transient Flow in Naturally Fractured Reservoirs and its Application to Devonian Gas Shales", paper SPE 9397, presented at the 55th Annual Fall Technical Conference and Exh. in Dallas, Tex, (Sep 21-24).

Kucuk, F. and Ayestaran, L., 1983*:* **"**Analysis of Simultaneously Measured Pressure and Sandface Flow Rate in Transient Well Testing"**,** paper SPE 12177 presented at the Annual Technical Conference and Exhibition, San Francisco, CA. Oct. 5-8.

Mavor, M. L. and Cinco Ley, H., 1979: "Transient Pressure Behavior of Naturally Fractured Reservoirs"**,** paper SPE 7977 presented at the Calif. Regional Meeting, Ventura, Ca., April 18-20.

Moench, A. F. and Ogata, A., 1984: "A Double Porosity Model for a Fissured Groundwater Reservoir with Fracture Skin", *Water Resources Research*, **Vol. 20**, No. 7, 831-846.

Najurieta, H. L., 1980: "A Theory for Pressure Transient Analysis in Naturally Fractured Reservoir", *J. Pet. Tech* (July), 1241- 1250.

Odeh, A. S., 1965: "Unsteady - State Behavior of Naturally Fractured Reservoirs", *Soc. Pet. Eng. J.* (March), *Trans*., AIME, **234,** 60-66.

Pirson, J. S., 1953: "Performance of Fractured Oil Reservoirs", Bull., AAPG, **Vol. 37**, 232-244.

Pollard, P., 1959: "Evaluation of Acid Treatments from Pressure Build-up Analysis", *Trans.*, AIME **216**, 38-43.

Rodríguez F.,Arana-Ortiz V. and Cinco Ley H., 2004: "Well Test Characterization of Small-and Large-Scale Secondary Porosity in Naturally Fractured Reservoirs", paper SPE 90287 presented at the Annual Technical Conference and Exhibition, Houston, Texas., September 26-29.

Sageev, A., Da Prat, G. and Ramey, H. J., 1985: "Decline Curve Analysis for Double Porosity Systems", paper SPE 13630 presented at the Annual Technical Conference and Exhibition, Bakersfield, CA., March 27-29.

Serra, K., Reynolds, A. C. and Raghavan, R., 1983: "New Pressure Transient Analysis Methods for Naturally Fractured Reservoirs", *J. Pet. Tech*. (Dec.) 2271-2284.

Stehfest, H., 1970: "Algorithm 368: "Numerical Inversion of Laplace Transforms", *Communications of the ACM* (Jan.) **13**, 47-49.

Stewart, G., Meunier D. and Wittman, M. J., 1983: "Afterflow Measurement and Doconvolution in Well Analysis"**,** paper SPE 12174 presented at the Annual Technical Conference and Exhibition, San Francisco, CA. Oct. 5-8.

Streltsova, T. D., 1976: "Hydrodynamics of Groundwater Flow in Fractured Formations", *Water Res. Research* (June), **Vol. 12**, No. 3, 405-414.

Streltsova, T. D., A., 1982: "Well Pressure Behavior of Naturally Fractured Reservoirs", paper SPE 10782, presented at the California Regional Meeting, San Francisco, Ca., March 24-26.

Strobel, C. J, Gulati, M. S. and Ramey, H. J., Jr., 1976: "Reservoir Limit Tests in a Naturally Fractured Reservoir- A Field Case Study Using Type Curves", *J. Pet. Tech.* (Sep.) 1097-1106.

de Swaan, O. A., 1976: "Analytical Solutions for Determining Naturally Fractured Reservoir Properties by Well Testing", April 2-4**,** *SPEJ* (June) 117-122; *Trans.*, AIME **261**.

Tsarevich, K. A. and Kuranov, I. F., 1956: "Calculation of the flow Rates for the Center Well in a Circular Reservoir Under Elastic Conditions", Problems of Reservoir Hydrodynamics, Leningrad, Part. 1, 9-34.

Uldrich, D. O. and Ershaghi, I., 1979: "A Method for Estimating the Interporosity Flow Parameter in Naturally Fractured Reservoirs", *Soc. Pet. Eng. J.* (Oct.) 324-332.

Van Everdingen, A. F. and Hurst,W., 1949: "The Application of the Laplace Transform to Flow Problems in Reservoirs", *Trans.,* AIME **186**, 305-324.

Warren, J. E. and Root, P. J., 1963: "The Behavior of Naturally Fractured Reservoirs", *Soc. Pet. Eng. J.* (Sep.), **Vol. 3**, 245-255; *Trans*. AIME, **228**.

Warren, J. E. and Root, P. J., 1965: "Discussion of Unsteady State Behavior of Naturally Fractured Reservoirs", *Soc. Pet. Eng. J.* (March) 64-65, *Trans*., AIME, **228,** 245-255.

NOMENCLATURE

A	= drainage area, ft^2.
B	= formation volume factor, RB/STB.
c_t	= compressibility, psi^{-1}.
C_A	= dimensionless pseudo steady state shape factor.
C_{fb}	= fracture area; is the ratio between matrix surface and rock volume, ft^{-1}.
h	= formation thickness, ft.
H	= matrix block size, ft.
In	= modified Bessel function, first kind, nth order.
k	= permeability, mD.
Kn	= modified Bessel function, second kind, nth order.
p	= pressure, psi.
$\bar{p}$	= Laplace transform of p .
p_{wf}	= wellbore flowing pressure, psi.
$q(t)$	= volumetric rate, bbl/day.
N_p	= cumulative production, bbl.
n	= number of normal set of fractures.
r_D	= dimensionless radius.
r_e	= outer boundary radius, ft.
r_{eD}'	= effective dimensionless well outer radius.
r_w	= wellbore radius, ft.
r_w'	= effective wellbore radius, ft.
s	= Laplace space parameter.
S_f	= fracture skin.
S_w	= Van Everdingen and Hurst skin factor.
t	= time, hours.
t_{DA}	= dimensionless time based on drainage area A.
V	= ratio of total volume of medium to bulk volume.
x	= thickness, ft.
α	= interporosity flow shape factor, ft^{-2}.
ς	= characteristic dimension of the heterogeneous medium, ft.

λ = dimensionless matrix-fracture permeability ratio, reflects the intensity of the fluid transfer matrix-fractures.

η = diffusivity.

μ = viscosity, cp.

ϕ = porosity, fraction.

ω = dimensionless fracture storativity, is the ratio of the storage capacity of the fracture to the total capacity of the medium.

SUBSCRIPTS

b = bulk (matrix and fractures).
D = dimensionless.
d = damaged zone.
e = external.
f = microfracture
F = fracture
m = matrix
surf = matrix-fracture surface
t = total

ACKNOWLEDGMENTS

Our appreciation to Enrique Ortuño M. for his constructive comments and reviews.

Appendix A. General and Approximate Solutions for the Transient Flow of a Fluid in a Naturally Fractured Reservoirs, with Transient.

Applying the transform to matrix-fracture function:

$$\bar{F}(\eta_{mFD},s)=L\left[4\eta_{mFD}\sum_{n=0}^{\infty}e^{-\eta_{mFD}(2n+1)^2\pi^2 t_D}\right]=4\eta_{mFD}\sum_{n=0}^{\infty}\frac{1}{s+\eta_{mFD}(2n+1)^2\pi^2} \quad \text{(A-1)}$$

The is Summatory in Eq. (A-1) can be represented by a continuous function:

$$\sum_{n=0}^{\infty}\frac{1}{s+\eta_{mFD}(2n+1)^2\pi^2}=\frac{1}{4}\frac{1}{\sqrt{s/\eta_{mFD}}}\left[\tanh\left(\frac{\sqrt{s/\eta_{mFD}}}{2}\right)\right] \quad \text{(A-2)}$$

Applying the transform microfracture-fracture:

$$\bar{F}_{mF}(\eta_{fFD},s)=L\left[4\eta_{fFD}\sum_{n=0}^{\infty}e^{-\eta_{fFD}(2n+1)^2\pi^2 t_D}\right]=4\eta_{fFD}\sum_{n=0}^{\infty}\frac{1}{s+\eta_{fFD}(2n+1)^2\pi^2} \quad \text{(A-3)}$$

Summatory can be represent by continuous function:

$$\sum_{n=0}^{\infty}\frac{1}{s+\eta_{fF_{mD}}(2n+1)^2\pi^2}=\frac{1}{4}\frac{1}{\sqrt{s/\eta_{fF_{mD}}}}\left[\tanh\left(\frac{\sqrt{s/\eta_{fF_{mD}}}}{2}\right)\right] \quad \text{(A-4)}$$

Applying the Laplace transform to Eq. (1) that describes the radial flow in the large scale secondary porosity media:

$$\frac{d^2\overline{p_{FD}}(r_D,s)}{dr_D^2}+\frac{1}{r_D}\frac{d\overline{p_{FD}}(r_D,s)}{dr_D}$$

$$-\omega_f C_{fFbD}\left[s\overline{p_{FD}}(r_D,s)-p_{FD}(r_D,0)\right]\frac{\bar{F}_{fF}(\eta_{fFD},s)}{1+S_{fF}\bar{F}_{fF}(\eta_{fFD},s)}$$

$$-[1-\omega-\omega_F]C_{mFbD}\left[s\overline{p_{FD}}(r_D,s)-p_{FD}(r_D,0)\right]\frac{\bar{F}_{mF}(\eta_{mFD},s)}{1+S_{mF}\bar{F}(\eta_{mFD},s)}$$

$$=\omega_F\left[s\overline{p_{FD}}(r_D,s)-p_{FD}(r_D,0)\right] \quad \text{(A-5)}$$

Replacing the initial condition given by Eq. (9) in the right hand side of Eq. (A-5):

$$\frac{d^2\bar{p}_{FD}(r_D,s)}{dr_D^2}+\frac{1}{r_D}\frac{d\bar{p}_{FD}(r_D,s)}{dr_D}$$

$$-\omega_f C_{fFbD}\, s\bar{p}_{FD}(r_D,s)\frac{\bar{F}_{fF}(\eta_{fFD},s)}{[1+S_{fF}\bar{F}_{fF}(\eta_{fFD},s)]}$$

$$-\left[1-\omega_f-\omega_F\right]C_{mFbD}\, s\bar{p}_{FD}(r_D,s)\frac{\bar{F}_{mF}(\eta_{mFD},s)}{[1+S_{mF}\bar{F}_{mF}(\eta_{mFD},s)]}$$

$$=\omega_F s\bar{p}_{FD}(r_D,s)=s\bar{p}_{FD}(r_D,s) \quad \text{(A-6)}$$

Eq. (A-6) can be written as follows:

$$\frac{d^2\overline{p_{FD}}(r_D,s)}{dr_D^2}+\frac{1}{r_D}\frac{d\overline{p_{FD}}(r_D,s)}{dr_D}-sf(s)\overline{p_{FD}}(r_D,s)=0 \quad \text{(A-7)}$$

where:

$$f(s)=\omega_F+\omega_f C_{fFbD}\frac{\bar{F}_{fF}(\eta_{fFD},s)}{1+S_{fF}\bar{F}_{fF}(\eta_{fFD,S})}$$

$$+[1-\omega_f-\omega_F]C_{mFbD}\frac{\bar{F}_{mF}(\eta_{mFD,S})}{1+S_{mF}\bar{F}_{mF}(\eta_{mFD,S})} \quad \text{(A-8)}$$

The general solution of the equation of flow in the large scale secondary porosity medium is:

$$\bar{p}_{FD}(r_D,s)=AIo\left(r_D\sqrt{sf(s)}\right)+BKo\left(r_D\sqrt{sf(s)}\right) \quad \text{(A-9)}$$

Applying the Laplace transform to the boundary conditions given by Eqs (10) and (11):

$$\frac{d\bar{p}_{FD}(1,s)}{dr_D}=-\frac{1}{s} \quad \text{(A-10)}$$

$$\lim_{r_D \to \infty} \bar{p}_{FD}(r_D, s) = 0 \qquad \text{(A-11)}$$

The for Eqs. (A-9) to (A-11) gives the Laplace space dimensionless pressure in the large scale secondary porosity:

$$\bar{p}_{FD}(r_D, s) = \frac{1}{s\sqrt{sf(s)}} \frac{Ko\left(r_D\sqrt{sf(s)}\right)}{K_1\left(\sqrt{sf(s)}\right)} \qquad \text{(A-12)}$$

where:

$$f(s) = \omega_F + \omega_f C_{fFbD}\, g_1(s) + [1 - \omega_f - \omega_F]\, C_{mFbD}\, g_2(s) \qquad \text{(A-13)}$$

Where the parameters C_{mFbD} and C_{fFbD} are given by Eqs. (32) and (34), and the transient transfer functions including the skin are:

$$g_1(s) = \frac{\eta_{fFD}^{3/2} \tanh(0.5\sqrt{s/\eta_{fFD}})}{\sqrt{s} + S_{fF}\eta_{mD}^{3/2} \tanh(0.5\sqrt{s/\eta_{fFD}})} \qquad \text{(A-14)}$$

$$g_2(s) = \frac{\eta_{mFD}^{3/2} \tanh(0.5\sqrt{s/\eta_{mFD}})}{\sqrt{s} + S_{mF}\eta_{mFD}^{3/2} \tanh(0.5\sqrt{s/\eta_{mFD}})} \qquad \text{(A-15)}$$

The dimensionless wellbore pressure can be expressed considering $r_D = 1$ in Eq. (A-10):

$$\bar{p}_{FwD}(s) = \frac{1}{s\sqrt{sf(s)}} \frac{Ko\left(\sqrt{sf(s)}\right)}{K_1\left(\sqrt{sf(s)}\right)} \qquad \text{(A-16)}$$

where:

$$f(s) = \omega_F + \omega_f C_{fFbD} \frac{\eta_{fFD}^{3/2}}{\sqrt{s} + S_{fF}\eta_{mD}^{3/2}} + [1 - \omega_f - \omega_F]\, C_{mFbD} \frac{\eta_{mFD}^{3/2}}{\sqrt{s} + S_{mF}\eta_{mFD}^{3/2}} \qquad \text{(A-17)}$$

Complete Analytical Solution

The following Bessel function relations are valid for great arguments:

$$K_1\left(\sqrt{s[A]}\right) \approx \frac{1}{\sqrt{s[A]}} \qquad \text{(A-18)}$$

$$K_0\left(\sqrt{s[A]}\right) \approx -ln\left(\frac{e^{\gamma}}{2}\sqrt{s[A]}\right) \qquad \text{(A-19)}$$

Substituting the approximations given by Eqs. (A-18) and and (A-19) in Eq. (A-16):

$$\bar{p}_{FwD}(s) = \frac{-ln\left(\frac{e^{\gamma}}{2}\sqrt{sf(s)}\right)}{s} \qquad \text{(A-20)}$$

Arranging:

$$\bar{p}_{FwD}(s) = \frac{\frac{-1}{2} ln\left(\frac{e^{2\gamma}s}{4} f(s)\right)}{s} = \frac{-1}{2}\frac{ln\left(\frac{e^{2\gamma}s}{4}\right)}{s} + \frac{-1}{2}\frac{ln(f(s))}{s} \qquad \text{(A-21)}$$

$$\bar{p}_{FwD}(s) = \frac{-1}{2}\frac{ln\left(e^{2\gamma}s/4\right)}{s} \frac{ln\left(\omega_F + \omega_f C_{fFbD}\frac{\eta_{fFD}^{3/2}}{\sqrt{s}+S_{fF}\eta_{mD}^{3/2}} + [1-\omega_f-\omega_F]C_{mFbD}\frac{\eta_{mFD}^{3/2}}{\sqrt{s}+S_{mF}\eta_{mFD}^{3/2}}\right)}{s} \qquad \text{(A-22)}$$

$$\bar{p}_{FwD}(s) = \frac{-1}{2}\frac{ln\left(\frac{e^{2\gamma}s}{4}\right)}{s} + \frac{-1}{2}\frac{ln\left(\frac{A\omega_F + B + C}{A}\right)}{s}$$

where:

$$A = s + \left[S_{fF}\eta_{mD}^{3/2} + S_{mF}\eta_{mFD}^{3/2}\right]\sqrt{s} + S_{fF}S_{mF}\eta_{mD}^{3/2}\eta_{mFD}^{3/2}$$

$$B = \omega_f C_{fFbD}\eta_{fFD}^{3/2}\left[\sqrt{s} + S_{mF}\eta_{mFD}^{3/2}\right]$$

$$C = [1 - \omega_f - \omega_F]\, C_{mFbD}\eta_{mFD}^{3/2}\left[\sqrt{s} + S_{fF}\eta_{mD}^{3/2}\right] \qquad \text{(A-23)}$$

$$\bar{p}_{FwD}(s) = -\frac{1}{2}\frac{ln\left(e^{2\gamma}s/4\right)}{s} - \frac{1}{2}\frac{ln(A\omega_F + B + C)}{s} + \frac{1}{2}\frac{ln(A)}{s} \qquad \text{(A-24)}$$

<u>*The complete solution in real time is*</u>:

$$p_{FwD}(t_D) = \frac{1}{2}\left[ln(t_D) + 0.80907 + Ei\left(\frac{-S_{fF}t_D}{C_{fFbD}\eta_{fFbD}[1-\omega_f-\omega_F]}\right)\right] + \frac{1}{2}\left[-Ei\left(\frac{-S_{fF}t_D}{C_{fFbD}\eta_{fFbD}\omega_f[1-\omega_f-\omega_F]}\right) + Ei\left(\frac{-S_{mF}t_D}{C_{mFbD}\eta_{mFbD}[1-\omega_f-\omega_F]}\right)\right]$$

$$+\frac{1}{2}\left[-Ei\left(\frac{-S_{mF}t_D}{C_{mFbD}\eta_{mFbD}\left[1-\omega_f-\omega_F\right]^2}\right)\right] \quad \text{(A-25)}$$

Approximate Analytical solution for short times

For small arguments, the function $f(s)$ given by Eq. (A-17) can be expressed:

$$\lim_{s\to\infty} f(s)=\lim_{s\to\infty}\ \omega_F+\lim_{s\to\infty}\frac{[1-\omega]C_{FbD}}{4}\frac{\sqrt{\eta_{mD}}}{\sqrt{s}}\left[tanh\left(\sqrt{s/\eta_{mD}}\Big/2\right)\right]$$

$$+\lim_{s\to\infty}\frac{[1-\omega]C_{mFbD}}{4}\frac{\sqrt{\eta_{mFbD}}}{\sqrt{s}}\left[tanh\left(\sqrt{s/\eta_{mFbD}}\Big/2\right)\right]=\omega_F \quad \text{(A-26)}$$

Replacing is limit for the transfer function in the wellbore pressure given by Eq. (A-16):

$$\bar{p}_{FwD}(s)=\frac{1}{s\sqrt{s\omega_F}}\frac{K_0\left(\sqrt{s\omega_F}\right)}{K_1\left(\sqrt{s\omega_F}\right)} \quad \text{(A-27)}$$

The following approximations for the Bessel functions are valid for small arguments:

$$K_0\left(\sqrt{s\kappa}\right)\approx -ln\left(e^{\gamma}\sqrt{s\omega_F}\Big/2\right) \quad \text{(A-28)}$$

$$K_1\left(\sqrt{s\kappa}\right)\approx\frac{1}{\sqrt{s\omega_F}} \quad \text{(A-29)}$$

Replacing the approximations given by Eqs. (A-28) and (A-29) in Eq. (A-20):

$$\bar{p}_{FwD}(s)=\frac{-ln\left(\frac{e^{\gamma}}{2}\sqrt{s\omega_F}\right)}{s} \quad \text{(A-30)}$$

The inversion of Eq. (A-30) results in the solution for early times:

$$p_{FwD}(t_D)=\frac{1}{2}\left[ln\left(\frac{t_D}{\omega_F}\right)+0.80907\right] \quad \text{(A-31)}$$

Approximate Analytical solution for long times:

$$\lim_{s\to 0} f(s)=\lim_{s\to 0}\ \omega+\lim_{s\to 0}\frac{[1-\omega]C_{FbD}}{4}\frac{\sqrt{\eta_{mD}}}{\sqrt{s}}\left[tanh\left(\frac{\sqrt{s/\eta_{mD}}}{2}\right)\right] \quad \text{(A-32)}$$

For small arguments $\frac{\sqrt{s/\eta_{mD}}}{2}$:

$$\lim_{s\to 0} f(s)=\omega+\frac{[1-\omega]C_{FbD}}{8}\frac{\sqrt{\eta_{mD}}}{\sqrt{s}}\frac{\sqrt{s}}{\sqrt{\eta_{mD}}}\ \approx \quad \text{(A-33)}$$

Replacing the is limit given by Eq. (A-32) in the wellbore pressure:

$$\bar{p}_{FwD}(s)=\frac{1}{s\sqrt{s}}\frac{K_0\left(\sqrt{s}\right)}{K_1\left(\sqrt{s}\right)} \quad \text{(A-34)}$$

The following approximations for the Bessel functions are valid for small arguments:

$$K_0\left(\sqrt{s}\right)\approx -ln\left(e^{\gamma}\sqrt{s}\Big/2\right) \quad \text{(A-35)}$$

$$K_1\left(\sqrt{s\kappa}\right)\approx\frac{1}{\sqrt{s\kappa}} \quad \text{(A-36)}$$

Substituting Eqs. (A-35) and (A-36) in Eq. (A-16):

$$\bar{p}_{FwD}(s)=\frac{-ln\left(e^{\gamma}\sqrt{s\kappa}\Big/2\right)}{s} \quad \text{(A-37)}$$

The inversion of this expression results in Eq. (A-38):

$$p_{FwD}(t_D)=\frac{1}{2}\left[ln(t_D)+0.809071\right] \quad \text{(A-38)}$$

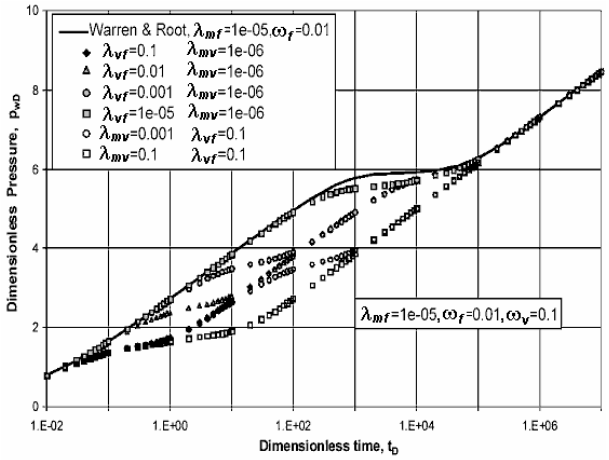

Fig. 1. Wellbore Transient Behavior, Unconnected microfractures, Constant Rate

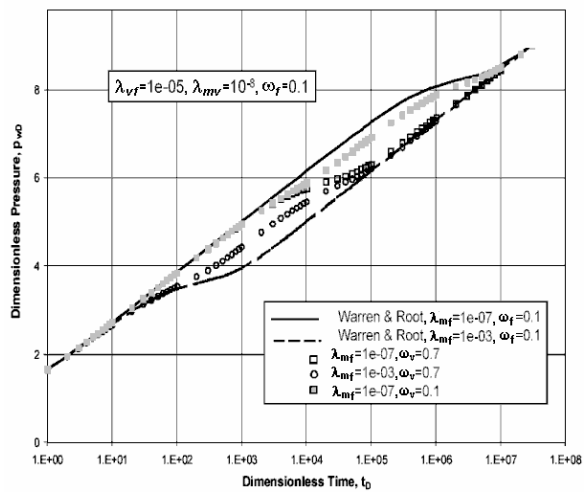

Fig. 2. Wellbore Transient Pressure, Constant Flow rate.

Error!

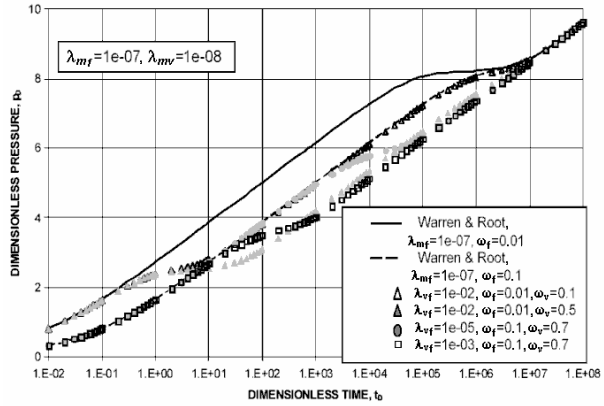

Fig. 3. Wellbore Transient Pressure Behavior, Unconnected Microfractures, Constant Flow rate.

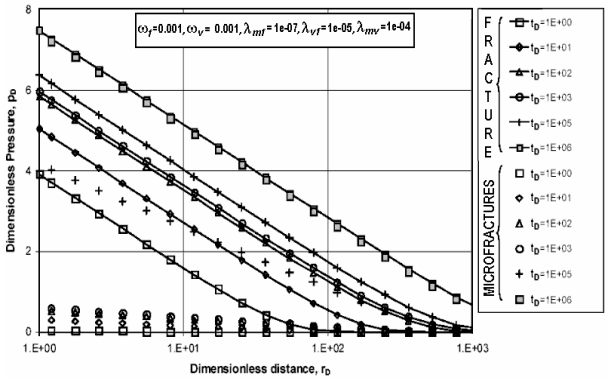

Fig. 4. Numerical Simulation Transient Pressure Profiles for Fractures and Microfractures Constant Flow rate.

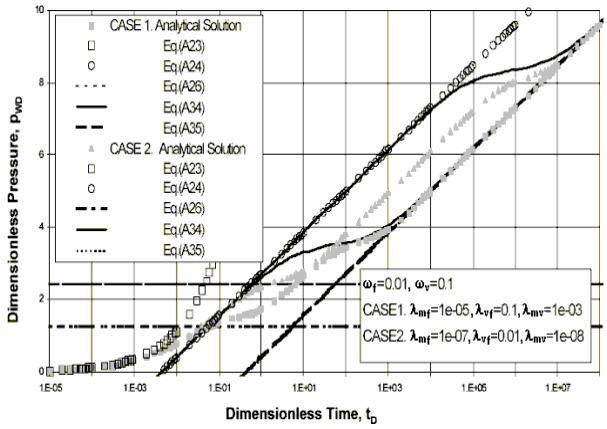

Fig. 5. Short, Intermediate, and Long Time Approximation,Unconnected microfractures.

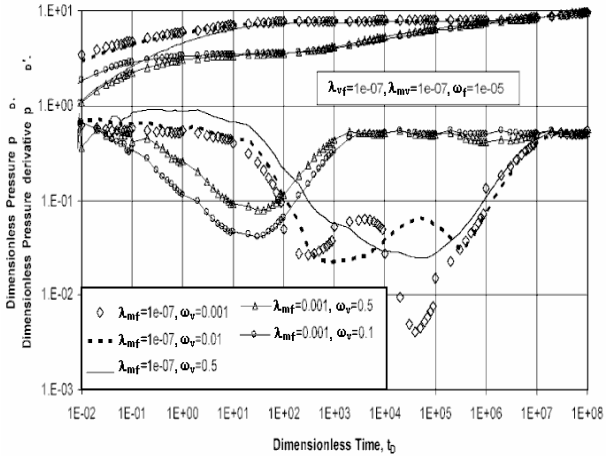

Fig. 6. Type Curve for Unconnected Microfractures

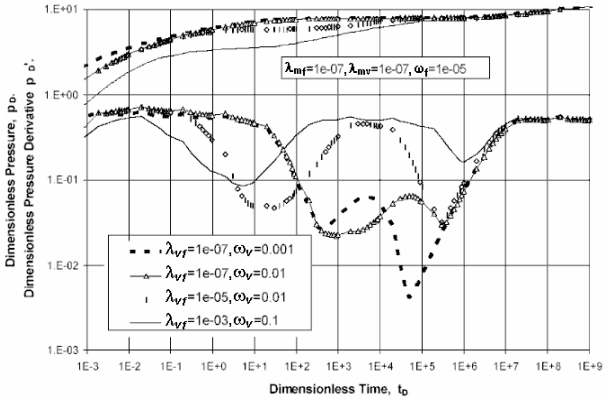

Fig. 7. Transient Type Curve for Unconnected microfractures, Constant Flow Rate.

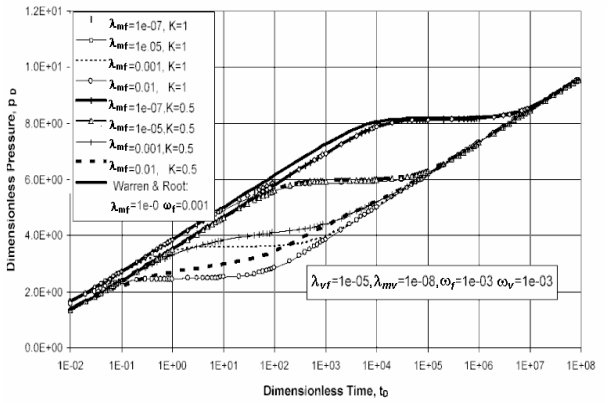

Fig. 8. Wellbore Transient Behavior, Connected (k<1) and Unconnected (k<1) microfractures, Constant Rate.

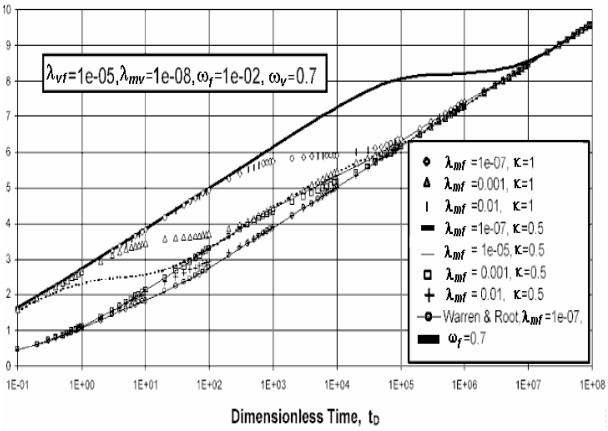

Fig. 9. Wellbore Transient Behavior, Connected and Unconnected microfractures, Constant Rate.

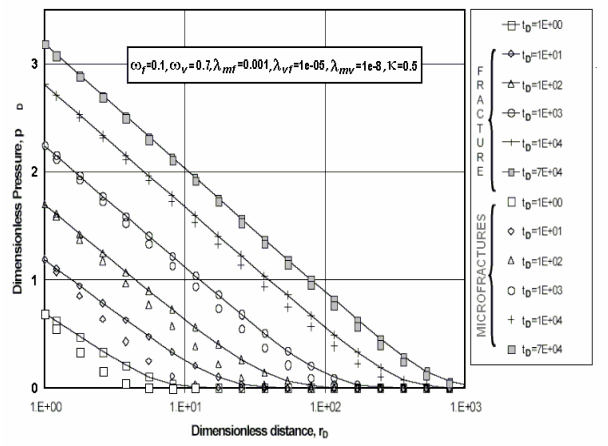

Fig. 10. Transient Pressure Profiles for microfractures and microfractures Networks Connected, Constant Flow Rate.